Kinetic and catalytic features of N-myristoyltransferases

Frédéric Rivière, Paul Monassa, Carmela Giglione, Thierry Meinnel

CHAPTER SIX

Kinetic and catalytic features of N-myristoyltransferases

Frédéric Rivière[iD,a,1,£], Paul Monassa[iD,a,£], Carmela Giglione[iD,@,a], Thierry Meinnel[iD,@,a,*]

[a] Université Paris Saclay, CEA, CNRS, Institute for Integrative Biology of the Cell (I2BC), 91198 Gif-sur-Yvette cedex, France

Running title: N-myristoyltransferase catalysis

Correspondence: carmela.giglione@i2bc.paris-saclay.fr (C. Giglione) or thierry.meinnel@i2bc.paris-saclay.fr (T. Meinnel)

[iD] ORCID iD 0001-6366-1904 (F. Rivière); ORCID iD 0003-4713-8069 (P. Monassa); ORCID iD 0002-7475-1558 (C. Giglione); ORCID iD 0001-5642-8637 (T. Meinnel)

[@]twitter @giglionelab (C. Giglione); @meinnel (T. Meinnel)

[£] These authors contributed equally

Present address

[1] Karolinska Institutet, Department of Biosciences and Nutrition, 14183 Huddinge, Sweden

Keywords: Protein acylation; lysine; myristoylation; acetylation; *N*-myristoyltransferase; N-terminus; glycine; enzyme kinetics.

Contents

Abstract

N-myristoyltransferases (NMTs) are members of the large family of GCN5-related N-acetyltransferases (GNATs). NMTs mainly catalyze eukaryotic protein myristoylation, an essential modification tagging protein N-termini and allowing successive subcellular membrane targeting. NMTs use myristoyl-CoA (C14:0) as major acyl donor. NMTs were recently found to react with unexpected substrates including lysine side-chains and acetyl-CoA. This chapter details the kinetic approaches that have allowed the characterization of the unique catalytic features of NMTs *in vitro*.

1. Introduction

Myristoylation describes a protein acylation that adds a fatty acid to the N-terminal glycines of ~2% of proteins in all eukaryotes (Castrec et al., 2018; Giglione & Meinnel, 2022; Lodge, Johnson, Weinberg, & Gordon, 1994; Meinnel, 2022; Meinnel, Dian, & Giglione, 2020; Pierre et al., 2007; Price et al., 2003). The lipid moiety anchors soluble proteins to internal membrane networks, where they interact with partners to initiate signal transduction (Bhatnagar, Ashrafi, Futterer, Waksman, & Gordon, 2001; Renna et al., 2013; Resh, 2006; Traverso et al., 2013b). N-myristoyltransferases (initially named glycylpeptide N-tetradecanoyltransferases, myristoyl CoA:protein N-myristoyltransferase, NMT; EC 2.3.1.97) are the only enzyme class known to catalyze myristoylation in eukaryotes and, given their central role in pathobiology, are promising therapeutic targets (Beauchamp et al., 2020; Frearson et al., 2010; Mousnier et al., 2018; Wright et al., 2014; Wright, Paape, Price, Smith, & Tate, 2016). NMTs were long thought to exclusively target proteins with an N-terminal glycine (Gly-myristoylation), usually through co-translational methionine excision (Kosciuk & Lin, 2020; Meinnel et al., 2020) or, less frequently, from post-translational cleavage

exposing new N-terminal glycines (Martin, Beauchamp, & Berthiaume, 2011; Thinon et al., 2014). More recently, several studies have indicated that both acetyl-CoA and lysine side chains can be used as CoA donors and targets, respectively.

A general scheme of classic NMT reactivity is provided in **Fig. 1A**. NMTs from *Arabidopsis thaliana* (AtNMT1), *Saccharomyces cerevisiae* (ScNMT), *Plasmodium falciparum* (PfNMT), or *Homo sapiens* (HsNMT1 and HsNMT2) have been studied *in vitro* using one or several such approaches (see references in (Giglione & Meinnel, 2022)). NMTs are members of the large GCN5-related N-acetyltransferase family, or GNATs (Bhatnagar et al., 1998). GNATs include many N-acetyltransferases modifying not only free amine groups on proteins (N-terminus and/or lysine side-chains) but also small metabolites including, for example, antibiotics (Salah Ud-Din, Tikhomirova, & Roujeinikova, 2016).

2. Materials, reagents, and buffers

2.1 Equipment

● 96-well plate reader, if possible equipped with two-way micro-injectors (Infinite M Nano+ plate reader, Tecan).

● Microplates for reading absorption: 96-well polystyrene clear flat-bottomed plates (Grenier Bio One, 655101; the optical path for 0.2 mL is 0.55 cm). It is possible to work with larger volumes up to 382 µl with these plates to increase signal, as the optical path increases proportionally (1 cm for 350 µL). Working with smaller amounts down to 100 µL may also be achieved (Grenier Bio One, 675101; the optical path for 0.1 mL is 0.58 cm).

● Microplates for fluorescence measurements, 96-well black solid-bottomed plates (Grenier Bio, 675076); working volume of 100 µL.

2.2 Enzymes

● Pyruvate dehydrogenase (PDH; 3.1.3.43 from porcine heart (Sigma-Aldrich P7032; 0.33 U/mg; >4 mg/ml), stored at -20°C. PDH catalyzes the reaction shown in **Fig. 1B.**

● HsNMT1, see details for preparation in Chapter 22 of this volume (Monassa et al., 2023).

● Full-length HsNMT2, AtNMT, PfNMT, and ScNMT can be expressed and purified according to similar protocols as described previously (Castrec et al., 2018; Traverso, Giglione, & Meinnel, 2013a).

● **Fig. S1** shows examples of purified NMT analysis by SDS-PAGE, where the purity is sufficient for kinetic studies.

2.3 Reagents

2.3.1 Fatty acyl derivatives

● Myristoyl-CoA lithium salt (Sigma-Aldrich, M4414) MM = 977.9 g/mol; 5 mg diluted in 25.565 mL. Stock solutions (0.2 mM) are prepared in 10 mM sodium acetate, pH 5.6, and 1% Triton X-100, except for MALDI analysis, where cholate is used instead of Triton to reduce background (see below). The low pH prevents slow CoA hydrolysis.

● Myristoyl-CoA lithium salt, 80% pure (Sigma-Aldrich, M4414) MM = 977.9 g/mol; 5 mg diluted in 0.511 mL in 50% DMSO (final concentration 10 mM).

● Acetyl-CoA, >93% pure (Sigma-Aldrich, A2056).

● Myristic acid (Sigma-Aldrich, M3128).

● Radioactive myristic acid, [1-^{14}C] or [9,10-^{3}H] (Moravek Inc., MC118 or MT918).

● Radioactive myristoyl-CoA is no longer available off-the-shelf from commercial suppliers. Unlike palmitate or stearate, which may be bought from Perkin-Elmer, for instance, radioactive myristate (^{3}H or ^{14}C) now needs to be ordered as a custom synthesis, e.g., from Selcia, Moravek Biochemicals Inc., Quotient Sciences, or ViTrax. It can also be prepared from radioactive

myristic acid and CoA according to the approach detailed in §3.1, Chapter 22, this volume. (Monassa et al., 2023)

2.3.2 Peptides

Polypeptides longer than six residues can be used for acylation reactions in the presence of an acyl donor (Kaplan, Mardon, Bishop, & Varmus, 1988; Towler et al., 1987). Octapeptides are optimal (see §3.4.2). Octapeptides bury all dedicated pockets of the binding site of NMTs (Meinnel et al., 2020).

● We order our custom octapeptides of any sequence from GenScript Biotech (Rijswijk, Netherlands), but peptides can also be ordered from many other companies worldwide. We typically order peptides (>5 mg net weight) with >95% purity delivered in three separate vials to allow for solubility testing and quality controlling prior to experimental use, usually by MALDI-TOF/TOF mass spectrometry (see details in Chapter 22, this volume (Monassa et al., 2023) and (Rivière et al., 2022)). An example with the ARF6-derived octapeptide is given in **Fig. 2A,B**.

● Cys-containing peptides are prone to oxidation. Storing in oxygen-free conditions at -20°C is recommended if storing for months.

● Stock solutions (10-100 mM depending on the solubility) are solubilized in water and stored at -20°C. Very acidic or basic peptides can require buffering with 50 mM Tris-HCl, pH=7.5. DMSO solubilization of the dry powder is sometimes useful for hydrophobic peptides. However, DMSO has a negative impact on NMT rates and should not exceed 1%.

● Our reference peptides are (i) *Arabidopsis thaliana* SOS3-derived for Gly-myristoylation or Gly-acetylation (G(C or S)SVSKKK, SOS3) or GKSFSKPR (GK) and human ARF6-derived (GKSVLSKIF, ARF6); (ii) the N-acetylated versions of ARF6 (*ac*-GKSVLSKIF; *ac*-ARF6) or *ac*-KSFSKPR (*ac*K) for Lys-myristoylation.

2.3.3 Notes

Any acyl-CoA variant different from myristoyl-CoA can be synthesized *in vitro* from the corresponding fatty acid derivatives as detailed in §3.1, Chapter 22 of this volume (Monassa et al., 2023).

2.4 Buffer components

2.4.1 For storage at room temperature

● Tris-HCl stock 0.5 M pH 8 q.s. 0.5 L; MM = 121.14 g/mol; 30.285 g Tris base in 500 ml H_2O; HCl 37 % ≈ 5mL to be added to reach pH 8.0; check pH with a pH meter and again once back to room temperature.

● $MgCl_2$ stock 100 mM q.s. 50 mL; MM = 203.3 g/mol ($6H_2O$); 1.0165 g in 50 mL.

● Triton X-100 10% q.s. 15 mL; dilute use 1.5 mL Triton X-100 solution (Sigma-Aldrich, 93443)

● EGTA 19.3 mM q.s. 100 mL (MM = 380.35 g/mol). Add 0.734 g to 100 mL with 2 NaOH chips to reach pH 8 and allow complete solubilization.

● Enzyme dilution buffer is Tris 50 mM pH 8 1 mL, BSA (0.1 mg/mL) 100 µL, H_2O 8.9 mL.

2.4.2 For storage at 4°C

● Sodium pyruvate (Sigma-Aldrich, S-8636, 100 mM).

2.4.3 For storage at -20°C

● Bovine serum albumin (BSA, Sigma-Aldrich) 10 mg/mL q.s. 10 mL in H_2O; aliquots of 200 µL.

● Dithiothreitol (DTT) 6.4 mM q.s. 20 mL; MM = 154.25 g/mol, 19.74 mg in 20 mL H_2O; prepare aliquots of 500 µL.

● Sodium acetate 10 mM/TritonX-100 1% solution: add sodium acetate 10 mM q.s. 100 mL (82.03 mg acetate-Na (82.03 g/mol) in 100 mL H_2O, 1 mL Triton X-100; set to pH 5.6 with a few drops of acetic acid and NaOH. Aliquots of 2 mL can be prepared.

● Thiamine pyrophosphate (TPP) 20 mM q.s. 5 mL (Sigma-Aldrich, C8754); MM = 460.8 g/mol; 46.08 mg in H_2O. Aliquots of 200 µL are convenient.

● NAD 25 mM q.s. 20 mL, MM = 663.4 g/mol; NAD-free acid grade 1 (Roche, 10127973001), 331.7 mg in 20 mL H_2O. Aliquots of 2 mL are sampled.

3. Kinetic analysis

3.1 GNAT-specific kinetic properties and considerations

NMT was long thought to catalyze fatty acylation of only N-terminal glycine residues (Meinnel et al., 2020). Recent data have shown that NMTs - as most GNATs - may also use acetyl-CoA as an effective CoA donor (Meinnel, 2022; Su, Kosciuk, Yang, Price, & Lin, 2021) and lysine side chains for possible protein anchoring (Dian et al., 2020; Kosciuk et al., 2020; Rivière et al., 2022). The following methods allow kinetic characterization of all these reactions. Examples and ranges are provided in §3.4 for each reaction type.

3.2 Discontinuous assays

3.2.1 Radioactive labeling

NMT activity can be assayed in a discontinuous manner at 30°C mainly according to (Boisson & Meinnel, 2003) based on well-established protocols (King & Sharma, 1991; Raju & Sharma, 1999). In this assay, the peptide substrate needs to display a strong basic character with at least three Lys or Arg residues to tightly retain the peptide on anionic bead phospho-cellulose filter papers. A 3-Arg tail C-terminal tag is sufficient; note that the SOS3 derivative

198 is fine without any alteration due to its native 3-Lys tail. This is a limitation of this assay,
199 however, as the actual sequence of a putative peptide target can only rarely be assessed.
200 ● The assay is performed in Eppendorf tubes (25 µl final volume) containing 0.2 µCi (i.e.,
201 ~0.14 µM) [^{3}H]myristoyl–CoA (61 Ci/mmol), 5-1000 µM peptide, 40 mM Tris–HCl (pH 7.4),
202 0.5 mM EGTA, 4.5 mM 2-mercaptoethanol, and 0.5% Triton X-100.
203 ● The reaction is initiated by the addition of NMT diluted in 50 mM Tris–HCl, pH 8.0, 0.1%
204 Triton X-100, 0.1 mg/mL BSA.
205 ● Various incubation times are performed (i.e., for 3, 6, and 9 min) to check and deduce initial
206 velocities.
207 ● 0 min time points together with samples performed in the absence of peptide or enzyme are
208 mandatory to assess background signal.
209 ● Reactions are stopped by filtration through P81 phospho-cellulose (Whatman, no longer
210 available) or LSA-50 paper (Appelmans et al., 2021). The filters are then dried using a hair
211 drier for 30 s, washed three times with 25 mM Tris–HCl, pH 7.3, and finally further dried.
212 Radioactivity is detected by scintillation counting after addition of the scintillation solution
213 (OptiScint HiSafe; Perkin–Elmer).
214 ● Radioactivity-based kinetic assays are no longer recommended for various reasons including
215 product availability (radioactive myristoyl-CoA is no longer commercially available to our
216 knowledge and must be prepared; see §2.3.2), time consumption (due, for instance, to
217 discontinuous monitoring), cost, radioprotection/safety rules, and waste management of long-
218 lasting radiolabels such as ^{3}H and ^{14}C.

219 *3.2.2 HPLC assays*

220 Discontinuous assays based on high-performance liquid chromatography (HPLC) analysis
221 of the reaction of NMT with its substrates are available. Reaction product analysis and

quantification are based on the differential retention times of the acylated and unmodified peptides. The reaction is usually performed in 100 µL volumes and then quenched with one volume of acetonitrile. After centrifugation (20,000 x g, 10 min, 4°C), 190 µL of the supernatant is mixed to 10 µL trifluoroacetic acid (TFA) prior to HPLC loading. Analysis is achieved on C18 reverse-phase columns (100 Å; 150 x 24.6 mm) with acetonitrile inverse (100 to 0%) gradient elution in 0.1% TFA.

The assay was originally coupled with radioactive quantification of the collected fractions (Rudnick, Duronio, & Gordon, 1992). One main advantage of HPLC analysis over the assay based on paper filtration is that the peptide sequence does not need to be modified by adding a basic tag and that actual sequences can be directly challenged without any bias.

The HPLC assay can also be used in a non-radioactive manner by monitoring absorbance intensities at 280 nm if a tryptophan tag is added to the sequence. Tryptophan has a very high molar absorption coefficient at 280 nm (ε_{280}=5690 $M^{-1}.cm^{-1}$). For instance, the GKVLSKIFWW sequence was used for ARF6 kinetic analysis with HsNMTs (Kosciuk et al., 2020; Su et al., 2021). Tryptophan tagging obviously mitigates the main advantage of the HPLC assay. It also significantly adds hydrophobicity to the peptide, increasing problems with solubilization. Monitoring absorbance at 210-220 nm – a range arising from the peptide bonds - along the HPLC profile should reveal the reaction products. Although less sensitive (ε_{210}~100 $M^{-1}.cm^{-1}$), such detection is in keeping with the analysis of genuine peptides. Finally, product and substrate detection and characterization of the unmodified peptides can also be monitored by coupling liquid chromatography with mass spectrometry. Quantification of both substrates and products may be achieved by taking advantage of the total ion chromatograms associated with each species (Kosciuk et al., 2020).

3.3 Continuous assays

Continuous assays have many advantages (speed, reliability, sensitivity, automatization, high-throughput) but need to be conducted with great care and mindful of several caveats (see §4.3.3). For instance, an NMT assay based on 5,5′-dithiobis-(2-nitrobenzoic acid) (Ellman's reagent, DTNB) thiol reactivity with CoA – the second product of the reaction – is accompanied by enzyme inhibition (Rudnick et al., 1992). Some multi-coupled assays aiming to detect CoA by following NADPH-coupled formation have been established (Farazi, Manchester, & Gordon, 2000). Here we describe a robust assay based on a unique coupling enzyme, pyruvate dehydrogenase (PDH), and NADH detection (Boisson & Meinnel, 2003; Traverso et al., 2013a).

3.3.1 NMT activity coupling conditions

NMT is assayed by continuously monitoring the formation of NADH by either absorbance at 340 nm or fluorescence (λ_{exc}=340 nm, λ_{em}=465 nm) in a coupled assay exploiting PDH activity (**Fig. 1B**). Coupling with PDH takes advantage of the second product of the reaction (CoA) to transform NAD into NADH. Signal detection originates from the high hyperchromicity of NADH at 340 nm with respect to NAD. Given the coupling scheme, one NADH molecule produced corresponds to one polypeptide acylation. The coupling does not provide direct information on the actual location of the modification on the polypeptide. MS approaches involving MS/MS modes are required for this purpose (**Fig. 2**, see §4.2, Chapter 22, this volume (Monassa et al., 2023)).

● NMT activity is assayed at 30°C in a reaction mixture containing 50 mM Tris-HCl (pH 8.0), 1 mM $MgCl_2$, 0.193 mM EGTA, 0.32 mM DTT, 0.2 mM TPP, 2 mM pyruvate, 0.1 mg/mL BSA, 0.1% Triton X-100, 2.5 mM NAD^+, 0.125 units/mL porcine heart PDH (0.33 units/mg), 40 µM myristoyl-CoA, and 1-2000 µM peptide. A final volume of 100-200 µL is used in 96-

well plates. The reaction mixture is pre-incubated for 3 min at 30°C before starting the reaction by adding myristoyl-CoA (20 µL in a final volume of 100 µL from the 200 µM stock). These parameters avoid problems arising from the solubility of the acyl-CoA derivative.

● The following parameters are given to the plate reader: temperature, 30 ± 0.5ºC; excitation wavelength, 340 nm (bandwidth 9 nm); emission wavelength, 465 nm (bandwidth 20 nm); reading mode, top; integration time, 20 µs; gain value, 100; sampling, 30 points per min (sequential mode), 3.3 points per min (parallel mode); number of reads, 25 (number of measures per well per cycle) for parallel mode, 3 for sequential mode, shaking before measurements, 3 sec (orbital) at 57 rpm.

3.3.2 Acylation kinetics

● NMT acylation reaction kinetics are monitored for 5-60 min, and the data are fitted to obtain the initial velocities associated with each peptide concentration. Initial velocities need to be carefully determined; due to establishing the coupling conditions over the very first time points, they can be underestimated and should not be taken into account before the coupling setting is properly balanced. Initial velocities are then measured with dozens of linear points. A value of 6300 $M^{-1}.s^{-1}$ is used as the molecular extinction coefficient of NADH at 340 nm for the absorbance assay. Initial rate values (v_i) expressed in $s^{-}1$ can be calculated as follows: v_i = slope/(60*261*[NMT]); the slope is in RFU/min and [NMT] is the final concentration of NMT in µM.

● Curve fits to obtain kinetic parameters are achieved by non-linear regression with GraphPad Prism 9.5.0 (GraphPad Software). Parameters with standard errors are computed for all parameters using the complete dataset including replicates. Both k_{cat} and K_m kinetic parameters are obtained by fitting to the Michaelis-Menten equation. A typical fit with three replicates is given in **Fig. 3A**. Fitting may use all values taken together or separately (**Fig. 3B**, out- and in-

sets). Averages and standard deviations (SDs) of the kinetic parameters are either the result of the fit with all values or from classic averaging approaches from different fits. k_{cat}/K_m values and the associated SDs can also be obtained by taking advantage of the k_{SP} approach (Johnson, 2019) with $k_{SP}=k_{cat}/K_m$ and $v_0/[E]= k_{SP}[S]/(1+[S]/K_m)$, where v_0 is the reaction rate measured at NMT concentration $[E_0]$. k_{cat}/K_m SD can also be calculated as follows from mean values of k_{cat} and K_m and their associated SDs: $SD(k_{cat}/K_m)= k_{cat}/K_m[(SD(K_m)/K_m)^2+(SD(k_{cat})/k_{cat})^2]^{1/2}$.

3.3.3 Notes

● NMTs use a sequential ordered Bi-Bi mechanism involving binding to the CoA derivative first and then to the peptidyl target (Rocque, Mcwherter, Wood, & Gordon, 1993; Rudnick et al., 1991; Salah Ud-Din et al., 2016).

● PDH-specific activity is sensitive to pH and only effective for coupling in the pH 7.5-9.0 range. The optimum pH of ScNMTs is 7.5-8.5, and HsNMT1 is only very active in the pH 7.0-9.0 range (Rocque et al., 1993). pH 8.0 is optimal for both PDH and NMT activities (**Fig. 4A**).

● Compared with Triton X-100, cholate reduces the NMT rate (**Fig. 4B**). Triton X-100 is therefore preferred for kinetic studies, while cholate is better suitable to MALDI approaches (see Chapter 22, this volume (Monassa et al., 2023)).

● Triton X-100 can be avoided when myristoyl-CoA is added to trigger the reaction if dissolved first in 50% DMSO as a 10 mM solution. The final DMSO concentration (0.2%) is low enough to not alter kinetics. This avoids the production of small bubbles that perturb signal monitoring, especially when using microinjectors.

● NADH fluorescence is often considered to be one magnitude more sensitive than absorbance (Rodriguez-Aparicio, Reglero, Martinez-Blanco, & Luengo, 1991). A main advantage of fluorescence assays is that they allow the determination of low K_m values, i.e., when their values are less than 10 µM. However, we have observed with the most recent PDH batches that

318 the signal-to-noise ratio is better with the absorbance-based assay. Unless the K_m value is lower
319 than 10 µM, we now prefer to use the absorbance assay.
320 ● **Fig. 3A** shows a representative fluorescence measurement series with the velocity in
321 RFU/min as a function of peptide concentration for one enzyme concentration. Curve fitting to
322 the Michaelis-Menten equation needs background velocity subtraction from each measurement
323 (see below). **Fig. 3B** shows a representative initial velocity relative to the peptide concentration
324 (expressed in s^{-1}).
325 ● Due to the coupling reaction, the initial velocity of NMT needs to be rate-limiting. This is
326 achieved if PDH is in sufficient excess (i.e., its steady-state rate is significantly higher than that
327 of NMT). For absorbance, we determined a 20 µM/min limit to the initial velocity measurement
328 (i.e., 0.13 A_{340}/min if the optical path is 1 cm). For fluorescence, we determined a similar limit
329 to the initial velocity measurement (i.e., 5,000 RFU/min, where RFU is relative fluorescence
330 unit). Exceeding this value, PDH is rate-limiting under our standard assay conditions, and NMT
331 must be diluted. The PDH concentration can be increased, but it is not recommended. In any
332 case, this needs to be experimentally verified in any new setting or with any new PDH batch.
333 ● In the fluorescence assay, concentrations of produced NADH higher than 30,000 RFU (115
334 µM) promote a non-linear response due to the inner filter effect of NADH at 340 nm.
335 Considering that 40 µM myristoyl-CoA and 100 µM acetyl-CoA correspond to standard
336 conditions, this issue only becomes relevant if these concentrations are increased above 115
337 µM.
338 ● The continuous assay is suited to high-throughput measurements in 96-well plates by
339 equipping the plate reader with microinjectors. Each well must first be filled with, for example,
340 a peptide sample with a multichannel pipette, which needs to be different or at different
341 concentrations. Next, microinjector A is used to fill each well with the reaction mixture but not
342 myristoyl-CoA. Microinjector B is used for robotic injection of myristoyl-CoA to start the

reaction. This allows multiple parallel kinetic acquisitions in short timeframes (**Fig. 3C**). Note that the dead volume of microinjectors is significant and it is therefore not recommended to use microinjectors to inject NMT directly if used at high concentrations and only available in limited amounts.

● The final concentration of myristoyl-CoA in the assay is 40 µM, which is the upper limit of solubility in the reaction mixture. This explains why, unusually, it is added to start the reaction, as it avoids intermediate higher concentrations. In its absence, because of the ordered Bi-Bi mechanism, the complex is not formed with the peptide. This myristoyl-CoA concentration is saturating for both ScNMT and AtNMT1 (Boisson & Meinnel, 2003) but not for HsNMTs, were the K_m values are one order of magnitude higher, i.e., 15 µM (Kishore et al., 1993).

● The 40 µM concentration of myristoyl-CoA limits the signal range to a maximum of 0.25 A_{340} per cm optical path when the peptide concentration is over 40 µM. When the peptide concentration is lower, the maximum range is directed by the peptide concentration itself. This needs to be taken into account in any analysis of the initial velocity slopes. With acetyl-CoA as the CoA donor, we use a 100 µM concentration, which can be extended to 150 µM (Asensio et al., 2022).

● Examples of kinetics and initial velocity curves are given in **Fig. 5**.

● When the NMT rate is low, the steady state is not immediately established and requires some time. Deriving the initial velocity therefore sometimes requires removing the first data points when the reaction is still being established (see **Fig. 5A,B**). This is classic in coupling reactions.

● In any case, the initial velocity (v_i) measured in the absence of peptide substrate is not zero (usually <50 RFU.min^{-1} or 0.001 A_{340}/min) and needs to be subtracted from the measured rate value (see **Fig. 5A**). This background partly comes from PDH, and its amplitude varies from one batch to another, eventually promoting slow NAD conversion into NADH and the signal

increases with incubation time. A reliable kinetic rate therefore needs to be significantly higher than this value. This can be achieved by increasing the enzyme concentration.

● When using microplates, as zeroing is not feasible for each well (see **Fig. 5A**), we recommend monitoring the kinetics in the absence of one component (e.g., NMT) for 15-30 minutes to determine both the intrinsic signal of each well and the associated inner drift. This likely involves slow CoA release due to chemical myristoyl- or acetyl-CoA hydrolysis in the slightly basic reaction buffer. The reader is then put on hold. After starting the kinetics with the missing component, the kinetics are then started again and monitored. This also allows the linking of the blank value determination with the kinetic signal and avoids any wrong interpretation if the kinetics are too fast, for instance. A typical procedure is shown in **Fig. 5A**.

● When the reaction is started with myristoyl-CoA, the slope of the reaction measured without the peptide is subtracted from those achieved in the presence of increasing peptide concentrations (**Fig. 5A**).

● We have noticed that initial velocities smaller than 0.001 µM.s^{-1} are difficult to precisely assess in routine practice. The K_m value range of most peptides measured to date is 5-200 µM.

3.4 Catalytic efficiencies of various substrates: ranges and meanings

3.4.1 CoA donors

Myristoyl-CoA is the best acyl donor. Other fatty acids can be used *in vitro* by NMT but with lesser efficiency. Myristate (C14:0) is a rather short fatty acid, and the dedicated fatty acyl binding site (pocket 1; (Meinnel et al., 2020)) acts as a sieve to prevent longer chains from efficiently binding to HsNMT1 (see Figure 5A in (Kishore et al., 1993)). Shorter fatty acids like C12:0 may bind, but the tension of the reactive thiolate between CoA and the fatty acid is important for achieving the reactive state. It has been reported that fatty acid derivatives shorter than C10 are not transferred onto protein targets.

Recent data have nevertheless shown that acetyl-CoA (a C2 derivative) can be a human NMT substrate (Su et al., 2021) with efficiency *in vitro* almost as strong as myristoyl-CoA. Specifically, the authors found that the catalytic efficiency (k_{cat}/K_m) for the CoA derivatives using ARF6 as the acylated peptide measured using an HPLC end-point assay were almost similar (See Table 1 in (Su et al., 2021)). The kinetic assay we report here in §3.3 was recently used for the assessment of GNAT activities using acetyl-CoA as the donor (Asensio et al., 2022). Using this kinetic assay to examine this reaction, we also observe this unexpected behavior of NMT, but with a catalytic efficiency two orders of magnitude lower than that observed in the previous report (**Fig. 6A-C**). This discrepancy comes from both the K_m and the k_{cat} values, which can be challenged by comparing the k_{cat}/K_m values relative to each substrate with both HsNMT1 and HsNMT2 (**Fig. 6D**). We also observed that the kinetic values with various peptides including ARF6 were again significantly different, and the reason for these inconsistences is unknown. It might be due to the presence of the di-tryptophan tag or the different temperatures used, i.e., 30°C *vs* 37°C. Regardless, MALDI MS/MS mass spectrometry unambiguously demonstrates full conversion and unambiguous acetylation of the N-terminus of the peptide substrate (**Fig. 2C,D**). Note that the MS/MS spectrum does not demonstrate in this case whether it involves Gly- or Lys-acetylation. An indirect proof of Gly- over Lys-acetylation may come from the study of the N-terminal acetylated version of the same peptide and demonstration that it cannot be acetylated further. This is the case for ARF6 acetylation, as the *ac*-ARF6 peptide - a peptide known to be acylated on the Lys amino group by HsNMT1 (Rivière et al., 2022) - is not acetylated by HsNMT1.

Finally, the physiological significance of the NMT-associated acetylation reaction *in cellulo* needs to be cautiously interpreted, as recently discussed (Meinnel, 2022). This is all the more true if kinetic data also contribute to disfavor - as we observe - acetyl-CoA over myristoyl-CoA.

3.4.2 Polypeptide acceptor donor

● Octapeptides are optimal and fully recapitulate not only the selectivity of NMT for Gly-myristoylation but also the kinetic parameters of a full-length protein (Boisson, Giglione, & Meinnel, 2003; Boisson & Meinnel, 2003; Rivière et al., 2022). In all cases, the kinetic parameters of Gly-myristoylation are remarkably similar to those of the full-length protein.

● Gly-myristoylation turnover number is low (~0.1 s^{-1}); this is the "price to pay" for the high selectivity of NMTs. K_m values of polypeptide substrates are in turn low (10 µM range) and are representative of the binding constant of the peptide (Meinnel, 2022).

● The catalytic efficiencies of Gly-myristoylation are on average of the order of 10^3-10^4 $M^{-1}.s^{-1}$. Nevertheless, the overall values obtained with octapeptides derived from genuine protein substrates which myristoylation was observed *in cellulo* is large, ranging from 10 to 10^5 $M^{-1}.s^{-1}$ (Castrec et al., 2018).

● Lys-myristoylation by NMT was recently shown to occur with a number of sequences provided they display the XKyySKy motif (Rivière et al., 2022), where X corresponds to 0-3 amino acids and y is any amino acid; the first Lys side chain is the recipient of the myristoylation (Dian et al., 2020; Kosciuk et al., 2020). To date, only ARF6 has been shown *in cellulo* to undergo secondary Lys-myristoylation on Lys3, but it needs first to undergo Gly-myristoylation on Gly2. The authors proposed that the Gly-myristoyl side chain can be embedded within the water channel to allow the second myristoyl-CoA to react (Kosciuk et al., 2020). A typical fit of Lys-myristoylation reactivity is shown in **Fig. 5D** with an N-acetylated version of ARF6. Catalytic performances of all tested Lys-myristoylation substrates are poor compared with Gly-myristoylation, mostly due to the very slow turnover number (k_{cat}) value (Rivière et al., 2022), which is two orders of magnitude lower and explains the 100-fold lower catalytic efficiencies of the two reactions. In fact, when the two reactions are feasible,

like for ARF6, Gly-myristoylation is always favored. A search for further substrates in humans failed (Rivière et al., 2022). For instance, peptide MKLRSKAA, derived from the N-terminus of human glucoside xylosyltransferase 2 (GXLT2), is not an HsNMT1 substrate *in vitro*.

4. Conclusions

In addition to the steady-state kinetic analysis presented in this chapter, pre-steady-state studies of NMTs using fast kinetic approaches requiring fluorescence-based stopped- or quenched-flow apparatus are available to derive finer details of the chemical mechanism and constants of NMTs (Farazi et al., 2000). This has provided the kinetic mechanism of ScNMT (see Figure 8 in (Farazi et al., 2000)). HsNMT and ScNMT share a similar mechanism (Rocque et al., 1993). A synthetic picture of the HsNMT catalytic mechanism is available (see Figure 1 in (Meinnel, 2022)). A unique feature of NMTs is that the rate limiting step of the reaction corresponds to the dissociation of the acylated peptide product (0.1 s^{-1}), whereas the chemical transformation is fast (>10 s^{-1}). This involves a conformational change (Dian et al., 2020).

Recent kinetic studies of NMTs have provided evidence that NMTs are very tightly linked to the GNAT family, not only through structural similarities of the common active site fold but also by their unique capacity to use acyl-CoA (including acetyl-CoA derivatives) on various amine reactive acceptor groups. This definitely integrates NMT - a previously unique outlier - within the GNAT family at the biochemical level. Another close example of similar performance is provided by a new family of plastid GNATs (Bienvenut et al., 2020; Giglione & Meinnel, 2021).

Acknowledgements

We acknowledge Benoit Castrec, Sara Ciccone, Rémy F. Dutheil, and José A. Traverso for their respective inputs in the setting of the various approaches presented in this manuscript.

Funding

This work was supported by French National Research Agency (ANR) DynaMYT (ANR-20-CE44-0013) and Fondation ARC (ARCPJA32020060002137) grants to TM. This work has benefited from the support of a French State grant (ANR-17-EUR-0007, EUR SPS-GSR) managed by the ANR under an Investments for the Future program (ANR-11-IDEX-0003-02). FR was supported by grants from Région Ile-de-France (17012695) and Fondation pour la Recherche Médicale (FDT202001010779).

References

Appelmans, O., Kashyap, R. S., Gilles, P., De Borggraeve, W. M., Voet, A., & Van Lint, J. (2021). LSA-50 paper: An alternative to P81 phosphocellulose paper for radiometric protein kinase assays. *Analytical Biochemistry, 630*, 114313.

Asensio, T., Dian, C., Boyer, J. B., Rivière, F., Meinnel, T., & Giglione, C. (2022). A continuous assay set to screen and characterize novel protein N-acetyltransferases unveils rice General Control Non-repressible 5-Related N-Acetyltransferase 2 activity. *Frontiers in Plant Science, 13*, 832144.

Beauchamp, E., Yap, M. C., Iyer, A., Perinpanayagam, M. A., Gamma, J. M., Vincent, K. M., et al. (2020). Targeting N-myristoylation for therapy of B-cell lymphomas. *Nature Communications, 11*, 5348.

Bhatnagar, R. S., Ashrafi, K., Futterer, K., Waksman, G., & Gordon, J. I. (2001). Biology and enzymology of protein N-myristoylation. In F. Tamanoi & D. S. Sigman (Eds.), *The Enzymes* (Vol. XXI (Protein lipidation), pp. 241-286). San Diego: Academic Press.

Bhatnagar, R. S., Futterer, K., Farazi, T. A., Korolev, S., Murray, C. L., Jackson-Machelski, E., et al. (1998). Structure of N-myristoyltransferase with bound myristoylCoA and peptide substrate analogs. *Nature Structural Biology, 5*, 1091-1097.

Bienvenut, W. V., Brünje, A., Boyer, J.-B., Mühlenbeck, J. S., Bernal, G., Lassowskat, I., et al. (2020). Dual lysine and N-terminal acetyltransferases reveal the complexity underpinning protein acetylation. *Molecular Systems Biology, 16*, e9464.

Boisson, B., Giglione, C., & Meinnel, T. (2003). Unexpected protein families including cell defense components feature in the N-myristoylome of a higher eukaryote. *Journal of Biological Chemistry, 278*, 43418-43429.

Boisson, B., & Meinnel, T. (2003). A continuous assay of myristoyl-CoA:protein N-myristoyltransferase for proteomic analysis. *Analytical Biochemistry, 322*, 116-123.

Castrec, B., Dian, C., Ciccone, S., Ebert, C. L., Bienvenut, W. V., Le Caer, J.-P., et al. (2018). Structural and genomic decoding of human and plant myristoylomes reveals a definitive recognition pattern. *Nature Chemical Biology, 14*, 671-679.

Dian, C., Pérez-Dorado, I., Rivière, F., Asensio, T., Legrand, P., Ritzefeld, M., et al. (2020). High-resolution snapshots of human N-myristoyltransferase in action illuminate a mechanism promoting N-terminal Lys and Gly myristoylation. *Nature Communications, 11*, 1132.

Farazi, T. A., Manchester, J. K., & Gordon, J. I. (2000). Transient-state kinetic analysis of Saccharomyces cerevisiae myristoylCoA:protein N-myristoyltransferase reveals that a step after chemical transformation is rate limiting. *Biochemistry, 39*, 15807-15816.

Frearson, J. A., Brand, S., McElroy, S. P., Cleghorn, L. A., Smid, O., Stojanovski, L., et al. (2010). N-myristoyltransferase inhibitors as new leads to treat sleeping sickness. *Nature, 464*, 728-732.

Giglione, C., & Meinnel, T. (2021). Evolution-driven versatility of N terminal acetylation in photoautotrophs. *Trends in Plant Science, 26*, 375-391.

Giglione, C., & Meinnel, T. (2022). Mapping the myristoylome through a complete understanding of protein myristoylation biochemistry. *Progress in Lipid Research, 85*, 101139.

Johnson, K. A. (2019). New standards for collecting and fitting steady state kinetic data. *Beilstein J Org Chem, 15*, 16-29.

Kaplan, J. M., Mardon, G., Bishop, J. M., & Varmus, H. E. (1988). The first seven amino acids encoded by the v-src oncogene act as a myristylation signal: lysine 7 is a critical determinant. *Molecular and Cellular Biology, 8*, 2435-2441.

King, M. J., & Sharma, R. K. (1991). N-myristoyl transferase assay using phosphocellulose paper binding. *Analytical Biochemistry, 199*, 149-153.

Kishore, N. S., Wood, D. C., Mehta, P. P., Wade, A. C., Lu, T., Gokel, G. W., et al. (1993). Comparison of the acyl chain specificities of human myristoyl-CoA synthetase and human myristoyl-CoA:protein N-myristoyltransferase. *Journal of Biological Chemistry, 268*, 4889-4902.

Kosciuk, T., & Lin, H. (2020). N-Myristoyltransferase as a glycine and lysine myristoyltransferase in cancer, immunity, and infections. *ACS Chem Biol, 15*, 1747-1758.

Kosciuk, T., Price, I. R., Zhang, X., Zhu, C., Johnson, K. N., Zhang, S., et al. (2020). NMT1 and NMT2 are lysine myristoyltransferases regulating the ARF6 GTPase cycle. *Nature Communications, 11*, 1067.

Lodge, J. K., Johnson, R. L., Weinberg, R. A., & Gordon, J. I. (1994). Comparison of myristoyl-CoA:protein N-myristoyltransferases from three pathogenic fungi:

Cryptococcus neoformans, Histoplasma capsulatum, and Candida albicans. *Journal of Biological Chemistry, 269*, 2996-3009.

Martin, D. D., Beauchamp, E., & Berthiaume, L. G. (2011). Post-translational myristoylation: Fat matters in cellular life and death. *Biochimie, 93*, 18-31.

Meinnel, T. (2022). Comment on "Binding affinity determines substrate specificity and enables discovery of substrates for N-Myristoyltransferases". *ACS Catalysis, 12*, 8195-8201.

Meinnel, T., Dian, C., & Giglione, C. (2020). Myristoylation, an ancient protein modification mirroring eukaryogenesis and evolution. *Trends in Biochemical Sciences, 45*, 619-632.

Monassa, P., Rivière, F., Dian, C., Frottin, F., Giglione, C., & Meinnel, T. (2023). Biochemical and structural analysis of N-myristoyltransferase-mediated protein tagging. *Methods in Enzymology, 686*, Chapter 22.

Mousnier, A., Bell, A. S., Swieboda, D. P., Morales-Sanfrutos, J., Perez-Dorado, I., Brannigan, J. A., et al. (2018). Fragment-derived inhibitors of human N-myristoyltransferase block capsid assembly and replication of the common cold virus. *Nature Chemistry, 10*, 599-606.

Pierre, M., Traverso, J. A., Boisson, B., Domenichini, S., Bouchez, D., Giglione, C., et al. (2007). N-Myristoylation regulates the SnRK1 pathway in Arabidopsis. *The Plant Cell, 19*, 2804-2821.

Price, H. P., Menon, M. R., Panethymitaki, C., Goulding, D., McKean, P. G., & Smith, D. F. (2003). Myristoyl-CoA:protein N-myristoyltransferase, an essential enzyme and potential drug target in kinetoplastid parasites. *Journal of Biological Chemistry, 278*, 7206-7214.

Raju, R. V., & Sharma, R. K. (1999). Preparation and assay of myristoyl-CoA:protein N-myristoyltransferase. *Methods in Molecular Biology, 116*, 193-211.

Renna, L., Stefano, G., Majeran, W., Micalella, C., Meinnel, T., Giglione, C., et al. (2013). Golgi traffic and integrity depend on N-myristoyl transferase-1 in Arabidopsis. *The Plant Cell, 25*, 1756-1773.

Resh, M. D. (2006). Trafficking and signaling by fatty-acylated and prenylated proteins. *Nature Chemical Biology, 2*, 584-590.

Rivière, F., Dian, C., Dutheil, R. F., Monassa, P., Giglione, C., & Meinnel, T. (2022). Structural and large-scale analysis unveil the intertwined paths promoting NMT-catalyzed lysine and glycine myristoylation. *Journal of Molecular Biology, 434*, 167843.

Rocque, W. J., McWherter, C. A., Wood, D. C., & Gordon, J. I. (1993). A comparative analysis of the kinetic mechanism and peptide substrate specificity of human and Saccharomyces cerevisiae myristoyl-CoA:protein N-myristoyltransferase. *Journal of Biological Chemistry, 268*, 9964-9971.

Rodriguez-Aparicio, L. B., Reglero, A., Martinez-Blanco, H., & Luengo, J. M. (1991). Fluorometric determination of phenylacetyl-CoA ligase from Pseudomonas putida: a very sensitive assay for a newly described enzyme. *Biochimica et Biophysica Acta, 1073*, 431-433.

Rudnick, D. A., Duronio, R. J., & Gordon, J. I. (1992). Methods for studying myristoyl-coenzyme A: protein N-myristoyltransferase. In N. M. Hooper & A. J. Turner (Eds.), *Lipid modification by proteins. A practical approach* (pp. 37-61). Oxford: IRL Press.

Rudnick, D. A., McWherter, C. A., Rocque, W. J., Lennon, P. J., Getman, D. P., & Gordon, J. I. (1991). Kinetic and structural evidence for a sequential ordered Bi Bi mechanism of catalysis by Saccharomyces cerevisiae myristoyl-CoA:protein N-myristoyltransferase. *Journal of Biological Chemistry, 266*, 9732-9739.

583 Salah Ud-Din, A. I., Tikhomirova, A., & Roujeinikova, A. (2016). Structure and functional
584 diversity of GCN5-related N-acetyltransferases (GNAT). *International Journal of*
585 *Molecular Sciences, 17*, E1018.
586 Su, D., Kosciuk, T., Yang, M., Price, I. R., & Lin, H. (2021). Binding affinity determines
587 substrate specificity and enables discovery of substrates for N-myristoyltransferases.
588 *ACS Catalysis, 11*, 14877-14883.
589 Thinon, E., Serwa, R. A., Broncel, M., Brannigan, J. A., Brassat, U., Wright, M. H., et al.
590 (2014). Global profiling of co- and post-translationally N-myristoylated proteomes in
591 human cells. *Nature Communications, 5*, 4919.
592 Towler, D. A., Adams, S. P., Eubanks, S. R., Towery, D. S., Jackson-Machelski, E., Glaser,
593 L., et al. (1987). Purification and characterization of yeast myristoyl CoA:protein N-
594 myristoyltransferase. *Proceedings of the National Academy of Sciences, 84*, 2708-2712.
595 Traverso, J. A., Giglione, C., & Meinnel, T. (2013a). High-throughput profiling of N-
596 myristoylation substrate specificity across species including pathogens. *Proteomics, 13*,
597 25-36.
598 Traverso, J. A., Micalella, C., Martinez, A., Brown, S. C., Satiat-Jeunemaitre, B., Meinnel, T.,
599 et al. (2013b). Roles of N-Terminal fatty acid acylations in membrane compartment
600 partitioning: Arabidopsis h-type thioredoxins as a case study. *The Plant Cell, 25*, 1056-
601 1077.
602 Wright, M. H., Clough, B., Rackham, M. D., Rangachari, K., Brannigan, J. A., Grainger, M.,
603 et al. (2014). Validation of N-myristoyltransferase as an antimalarial drug target using
604 an integrated chemical biology approach. *Nature Chemistry, 6*, 112-121.
605 Wright, M. H., Paape, D., Price, H. P., Smith, D. F., & Tate, E. W. (2016). Global profiling
606 and inhibition of protein lipidation in vector and host stages of the sleeping sickness
607 parasite Trypanosoma brucei. *ACS Infectious Diseases, 2*, 427-441.

608

609 **Figure Legends**

610 Fig. 1. Reactions catalyzed by the main enzymes useful for NMT studies. (A) NMT. (B) PDH.

611

612 Fig. 2. MALDI MS characterization of the modification state of an NMT substrate. MALDI-
613 TOF/TOF analysis of the GK peptide upon NMT acetylation. (A) MS analysis of the GK
614 peptide. (B) MS analysis of the HsNMT1-acetylated GK peptide. The 42 Da increment
615 compared with panel A is noticeable. (C) MS/MS analysis of the non-modified GK peptide.
616 (D) MS/MS analysis of the NMT-acetylated GK peptide.

617

618 Fig. 3. Continuous fluorescent kinetic analysis of Gly- and Lys-myristoylation by NMT. (A)
619 Rough initial velocity of myristoylation by AtNMT1 (expressed as RFU/min) as a function of
620 SOS3 peptide concentration. Three replicates are displayed. The background velocity in the
621 absence of peptide substrate (or of NMT) as shown here is 50 RFU/min. After subtracting the
622 background velocity kinetic, which cannot be neglected, parameters can be calculated. Here,
623 Vmax = 689±26 RFU/min; K_m = 18.0±2.6 µM. (B) Example of a classic kinetic analysis - here
624 of ARF6 Gly-myristoylation with HsNMT1 - showing the different modes of fitting, either
625 with all three replicates together or with distinct fits with each replicate (inset). Here, the values
626 are K_m=7.8±2.2 µM, k_{cat}=0.032±0.002 s^{-1}, k_{cat}/K_m=4121±948 $M^{-1}.s^{-1}$. (C) Example of a high-
627 throughput analysis of a 96-sample with a plate reader. The injectors allow robotic starts and
628 precise timing. The inset shows the overlay of all kinetics. Initial velocities need to be measured
629 at the early, linear stages. (D) Kinetics of Lys-myristoylation of *ac*-ARF6 showing the 2-order
630 of magnitude decrease in turnover number compared with Gly-myristoylation. Here,
631 K_m=17.0±4.8 µM, k_{cat}=0.00078±0.00004 s^{-1}, k_{cat}/K_m=43±7 $M^{-1}.s^{-1}$.

632

Fig. 4. Impact of various biochemical features on PDH and NMT activities. Gly-myristoylation of NMT was studied with peptide SOS3. (A) Impact of pH on PDH activity (grey) and ScNMT activity (data from Table 1 in (Towler et al., 1987)). (B) Impact of cholate on AtNMT1 activity.

Fig. 5. Examples of kinetics, initial velocity slopes, and relative fit to the Michaelis-Menten equations. Measurements are made on a plate reader. The sampling is 10 seconds. (A) SOS3 peptide (0 or 100 µM) Gly-myristoylation kinetics in the presence or absence of HsNMT1 (0.5 µM): a typical pipeline with various parts of the analysis is detailed. (B) Influence of GK peptide concentration on HsNMT2 acetylation with acetyl-CoA (100 µM). (C) Influence of acetyl-CoA peptide concentration on HsNMT1 acetylation with ARF6 (500 µM). (D) Fit to the Michaelis-Menten equation of the slopes of panel (C).

Fig. 6. NMT as an N-acetyl transferase *in vitro*. (A) Kinetics of Gly-acetylation of ARF6 by HsNMT1. The fit was made with the k_{SP} approach to yield K_m=106±22 µM, k_{cat}/K_m=27.5±4.3 $M^{-1}.s^{-1}$. (B) Michaelis-Menten assessment of the parameters of Acetyl-CoA. ARF6 peptide concentration was set at 500 µM, which corresponds to 82% of the maximum velocity. Higher concentrations are difficult to reach without bias. (C) Table of all parameters of Gly-acetylation by HsNMT1 and HsNMT2 with two peptides assayed at 100 µM acetyl-CoA, ARF6, and GK as determined with the continuous assay described in this manuscript. (D) Comparison of the acetylation performances (Catlaytic efficiency, k_{cat}/K_m) obtained by two independent teams and two different methods to determine the kinetic parameters. Data in black are associated to those of the other panel of this figure. The data in grey are from (Su et al., 2021); *NA*, data not available.

Supplementary Figure Legends

Fig. S1. Various purified versions of NMTs.

A

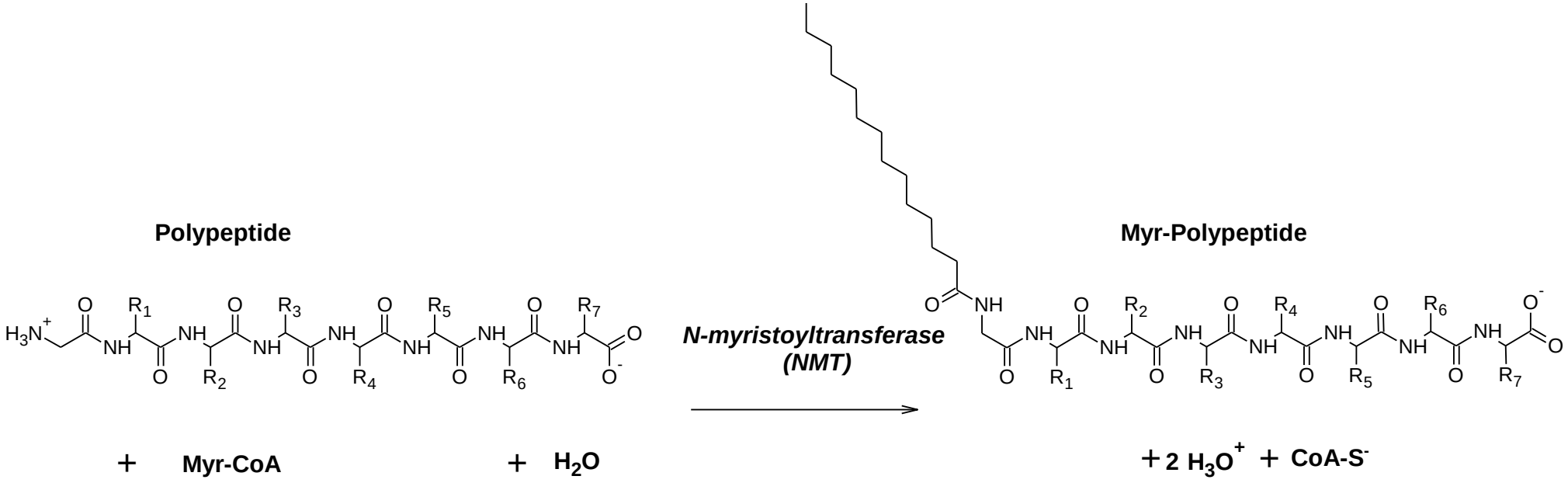
Polypeptide
Myr-Polypeptide
N-myristoyltransferase
(NMT)
+ Myr-CoA
+ H2O
+ 2 H3O+ + CoA-S-

B

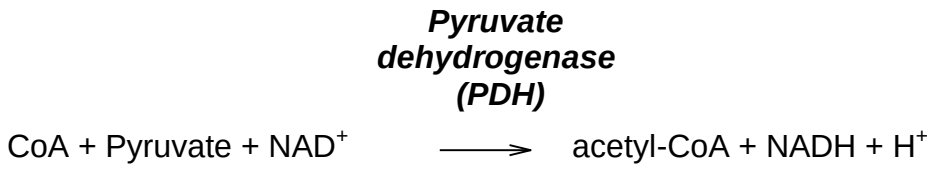
Pyruvate
dehydrogenase
(PDH)
CoA + Pyruvate + NAD+
acetyl-CoA + NADH + H+

Fig. 1

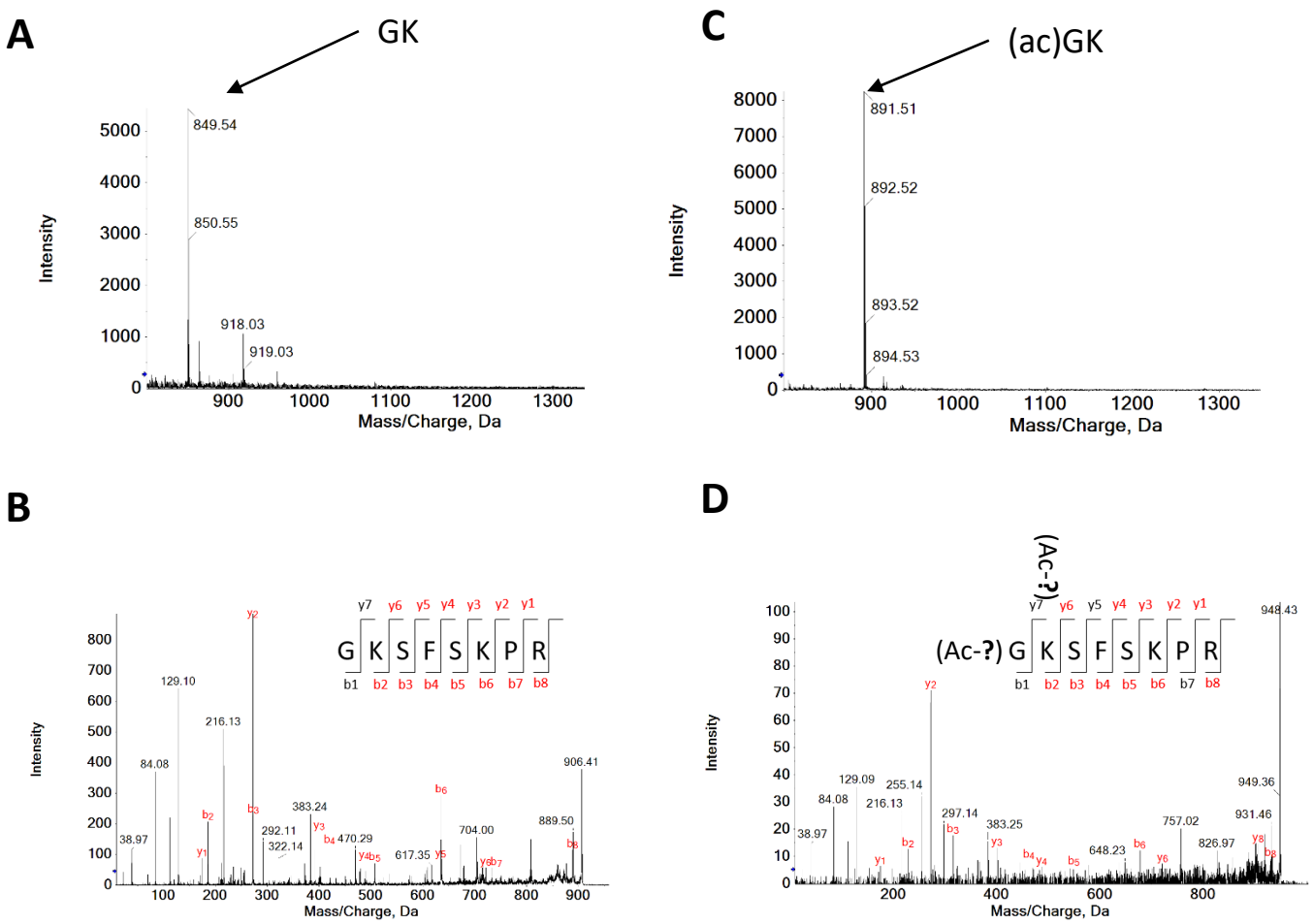
A
GK
849.54
850.55
918.03
919.03
Intensity
Mass/Charge, Da
C
(ac)GK
891.51
892.52
893.52
894.53
Intensity
Mass/Charge, Da
B
G K S F S K P R
b1 b2 b3 b4 b5 b6 b7 b8
y7 y6 y5 y4 y3 y2 y1
129.10
216.13
84.08
906.41
383.24
292.11
322.14
470.29
617.35
704.00
889.50
38.97
Intensity
Mass/Charge, Da
D
(Ac-?) G K S F S K P R
b1 b2 b3 b4 b5 b6 b7 b8
y7 y6 y5 y4 y3 y2 y1
948.43
949.36
931.46
757.02
826.97
648.23
383.25
297.14
255.14
129.09
216.13
84.08
38.97
Intensity
Mass/Charge, Da

Fig. 2

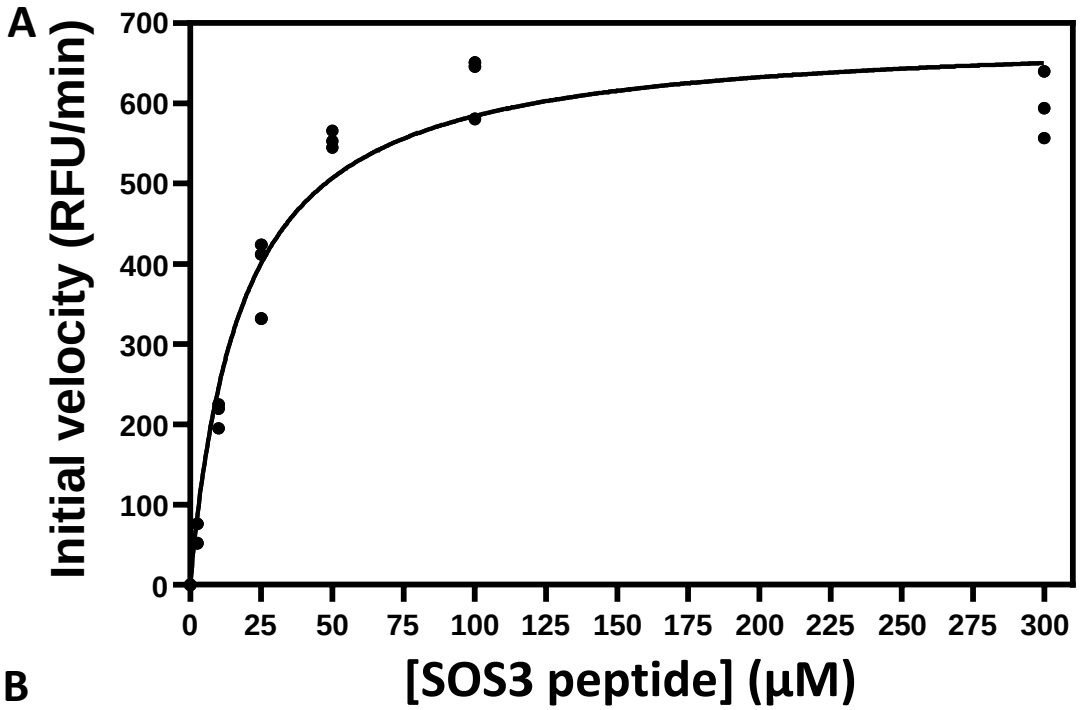
A
Initial velocity (RFU/min)
700
600
500
400
300
200
100
0
0 25 50 75 100 125 150 175 200 225 250 275 300
[SOS3 peptide] (μM)

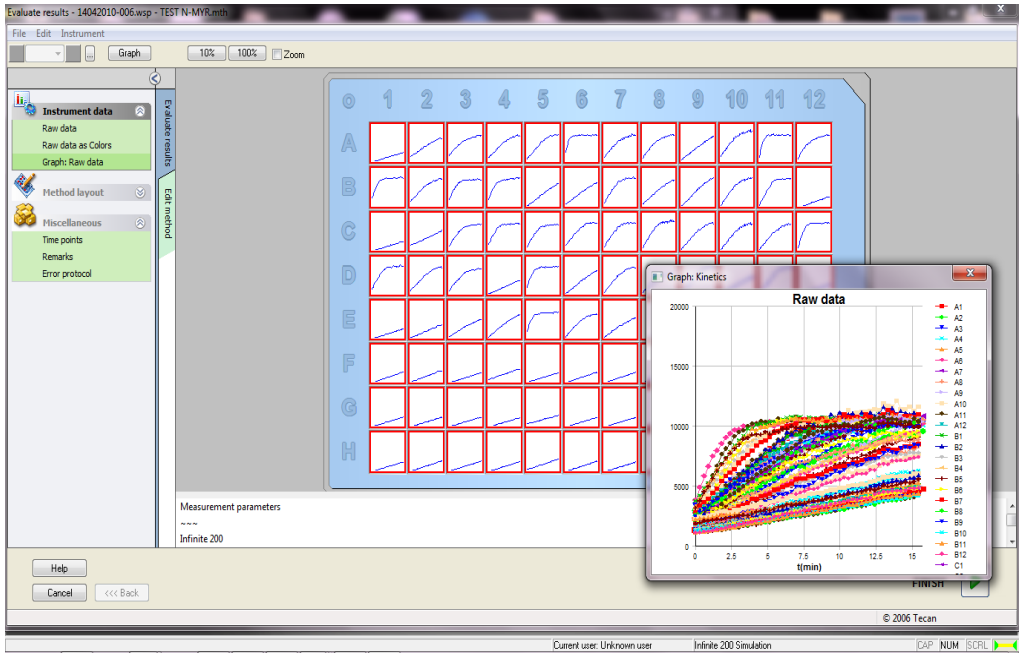
C
Graph: Kinetics
Raw data
Instrument data
Raw data
Raw data as Colors
Graph: Raw data
Method layout
Miscellaneous
Time points
Remarks
Error protocol
Measurement parameters
Infinite 200
Help
Cancel
© 2006 Tecan

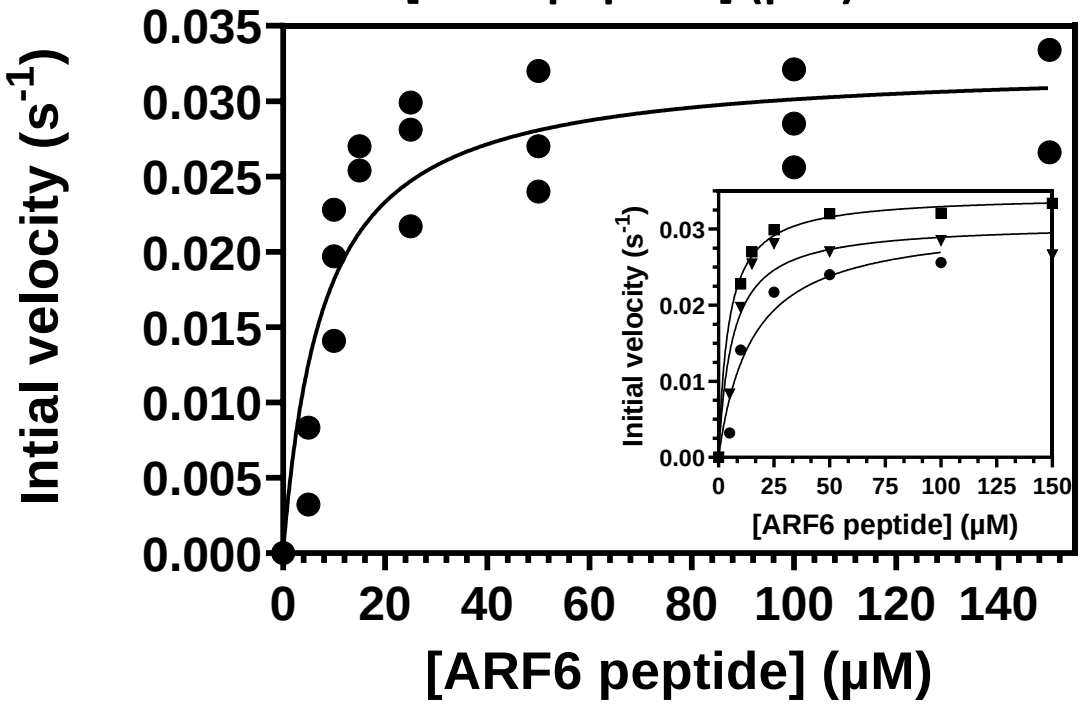
B
Intial velocity (s-1)
0.035
0.030
0.025
0.020
0.015
0.010
0.005
0.000
0 20 40 60 80 100 120 140
[ARF6 peptide] (μM)
Initial velocity (s-1)
0.03
0.02
0.01
0.00
0 25 50 75 100 125 150
[ARF6 peptide] (μM)

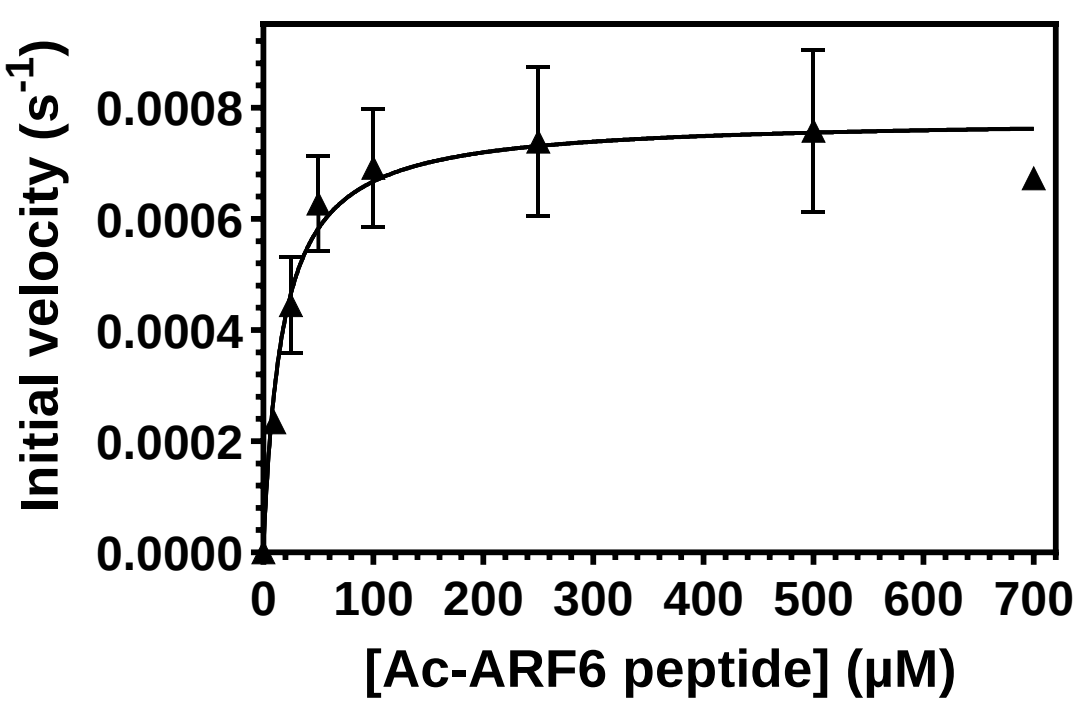
D
Initial velocity (s-1)
0.0008
0.0006
0.0004
0.0002
0.0000
0 100 200 300 400 500 600 700
[Ac-ARF6 peptide] (μM)

Fig. 3

A

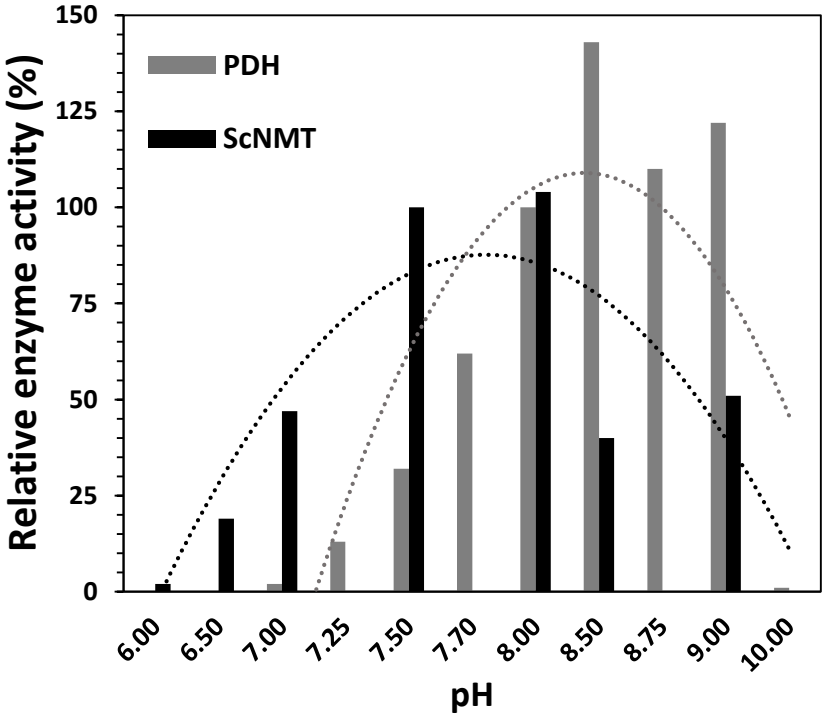
Relative enzyme activity (%)
150
125
100
75
50
25
0
PDH
ScNMT
6.00
6.50
7.00
7.25
7.50
7.70
8.00
8.50
8.75
9.00
10.00
pH

B

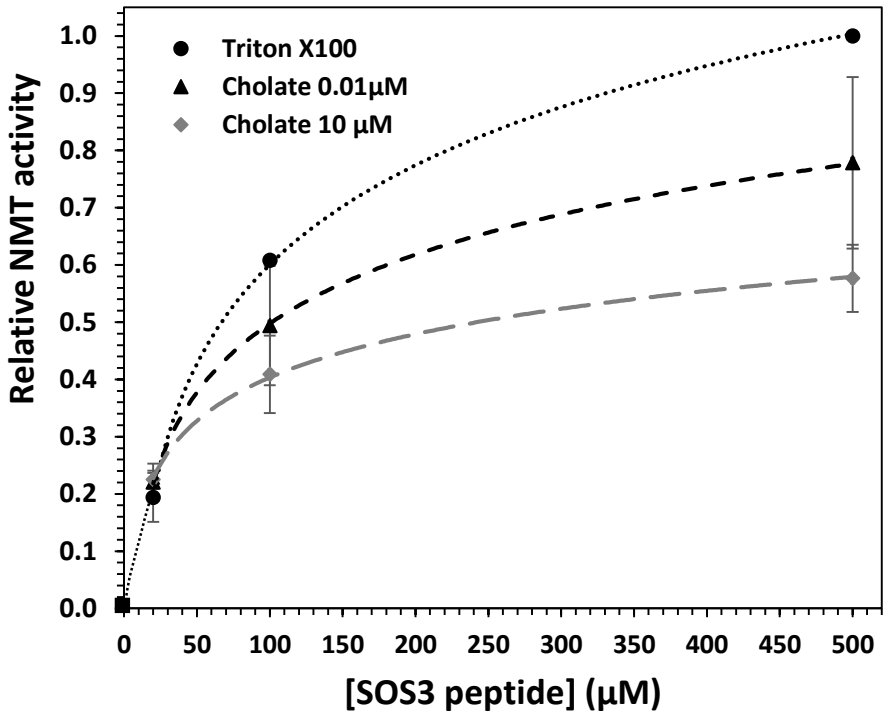
Relative NMT activity
1.0
0.9
0.8
0.7
0.6
0.5
0.4
0.3
0.2
0.1
0.0
Triton X100
Cholate 0.01µM
Cholate 10 µM
0
50
100
150
200
250
300
350
400
450
500
[SOS3 peptide] (µM)

Fig. 4

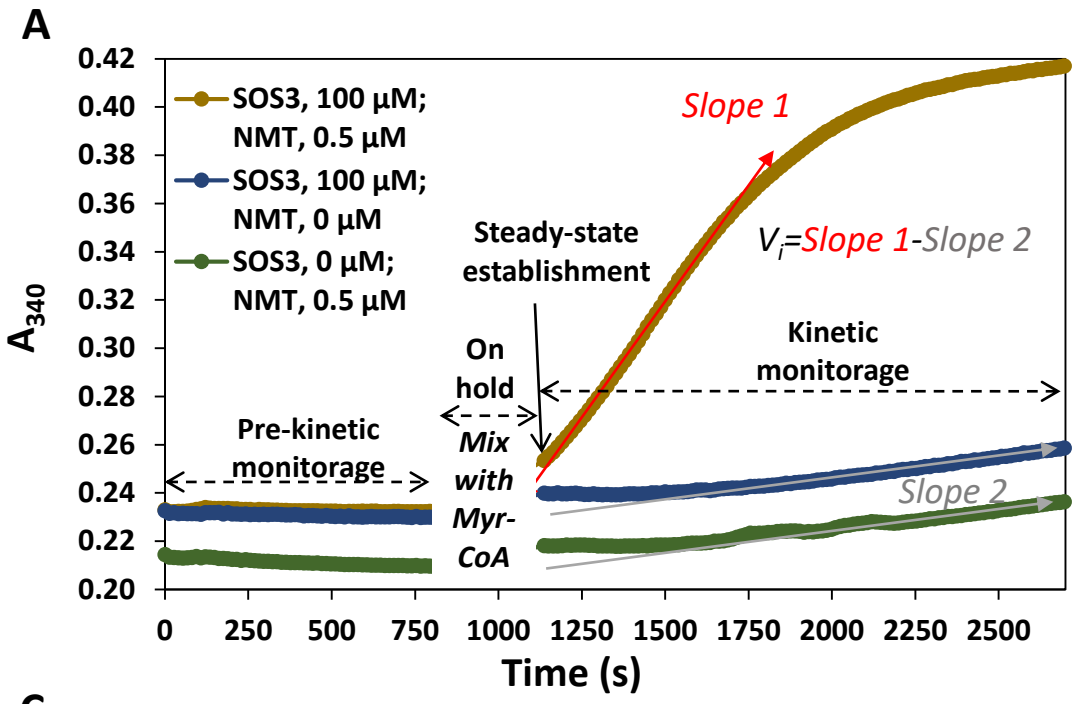
A
SOS3, 100 μM; NMT, 0.5 μM
SOS3, 100 μM; NMT, 0 μM
SOS3, 0 μM; NMT, 0.5 μM
Slope 1
Steady-state establishment
V_i=Slope 1-Slope 2
On hold
Mix with Myr-CoA
Kinetic monitorage
Pre-kinetic monitorage
Slope 2
A_{340}
Time (s)

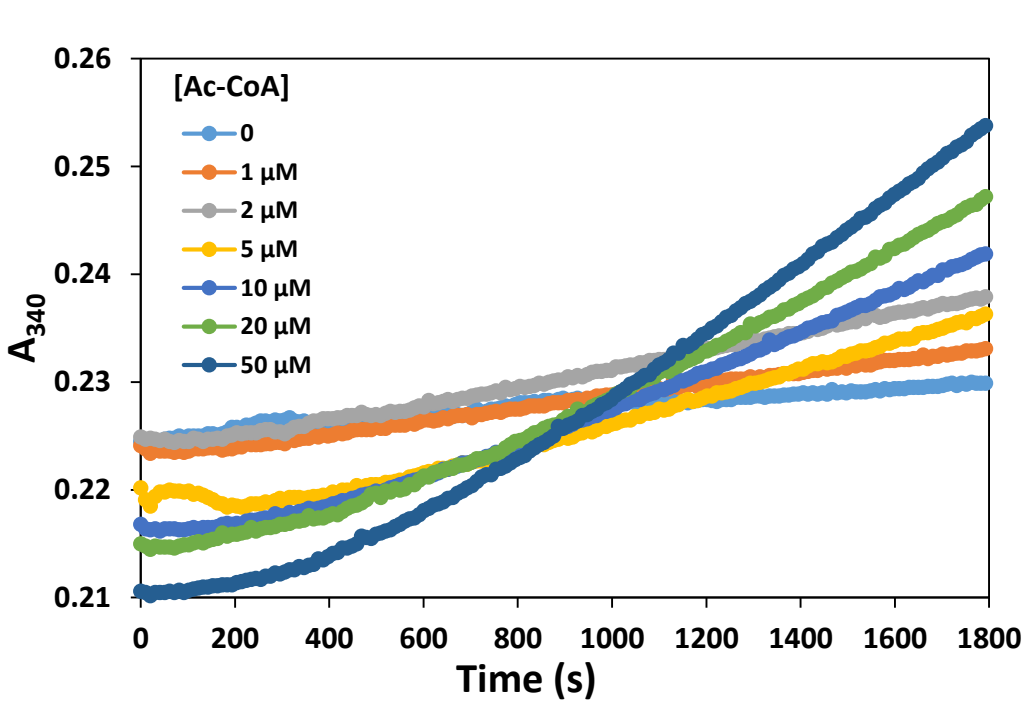
B
[Ac-CoA]
0
1 μM
2 μM
5 μM
10 μM
20 μM
50 μM
A_{340}
Time (s)

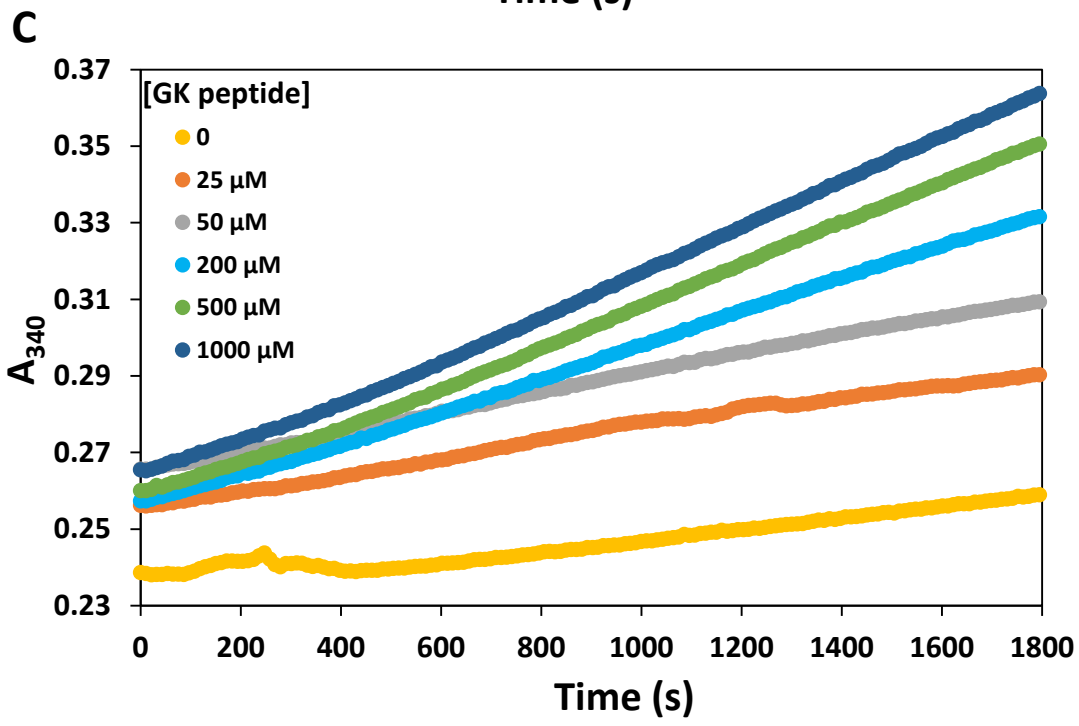
C
[GK peptide]
0
25 μM
50 μM
200 μM
500 μM
1000 μM
A_{340}
Time (s)

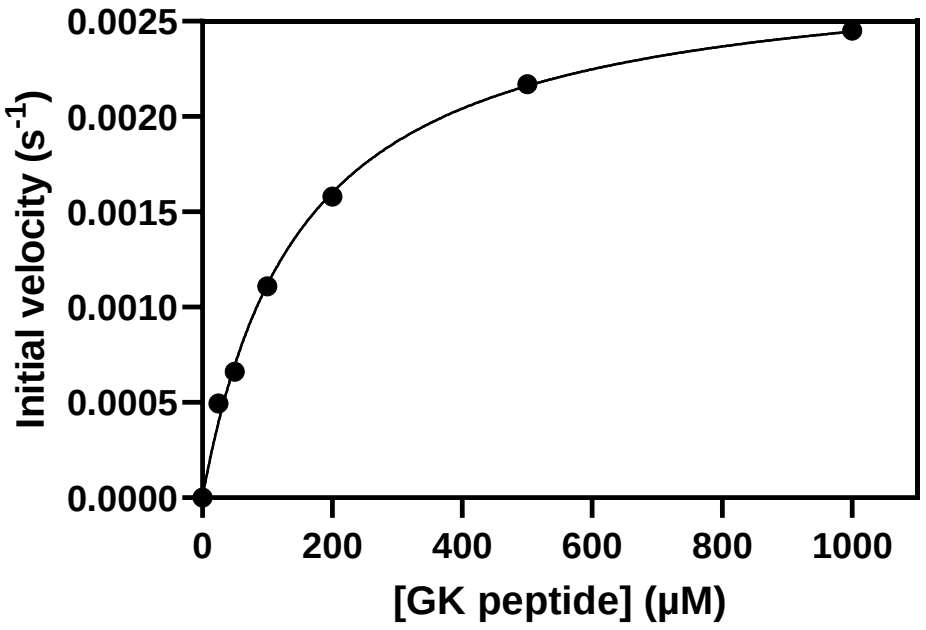
D
Initial velocity (s^{-1})
[GK peptide] (μM)

Fig. 5

A

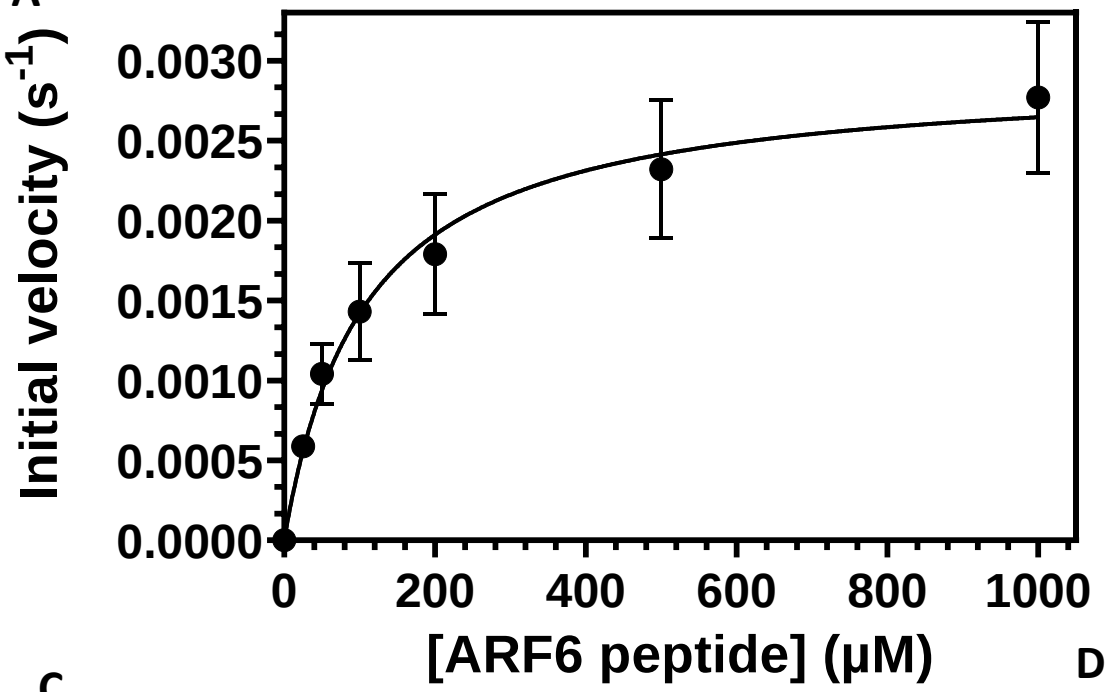

B

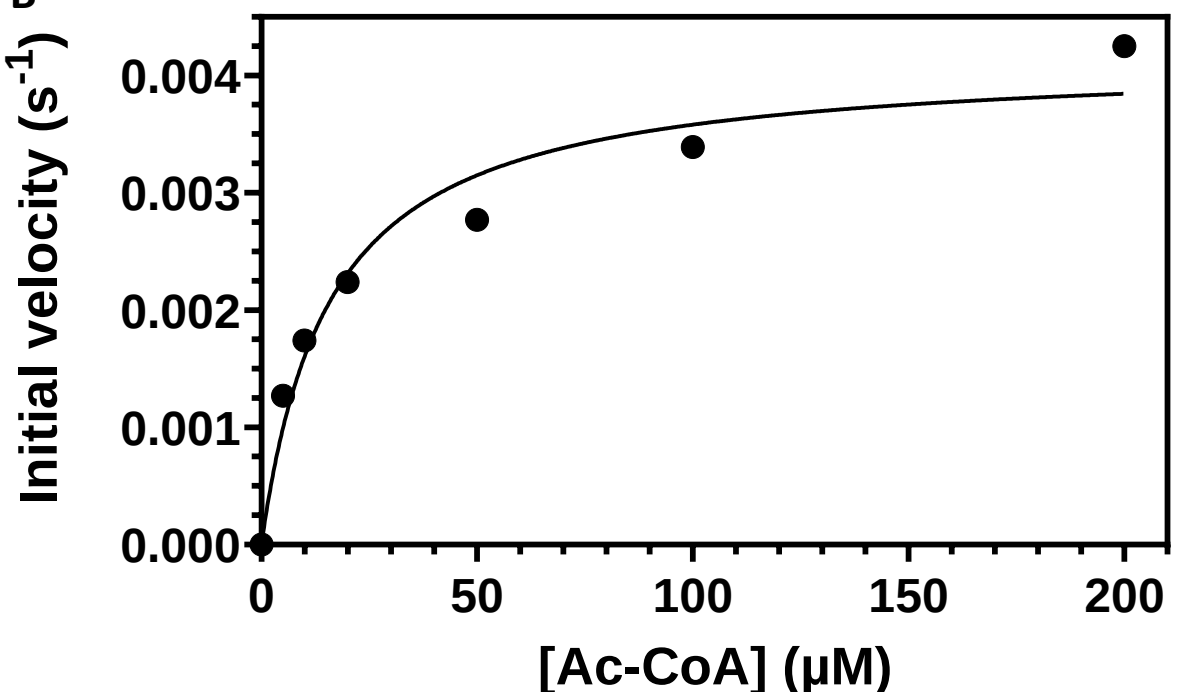

C

NMT	Kinetic parameter	Substrate	Value
HsNMT1	K_m (µM)	Ac-CoA	16 ± 4
		ARF6	106 ± 22
		GK	149 ± 22
HsNMT2			156 ± 18
HsNMT1	k_{cat} (s^{-1})	ARF6	0.0029 ± 0.0003
HsNMT1 &HsNMT2		GK	0.0029 ± 0.0004

D

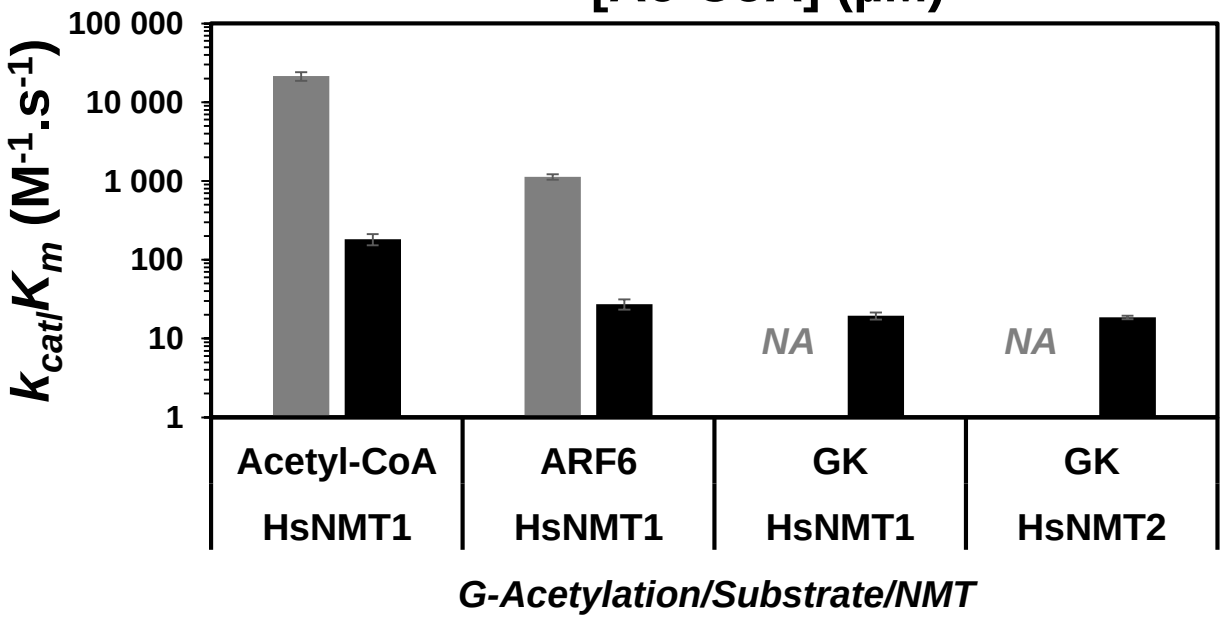

Fig. 6

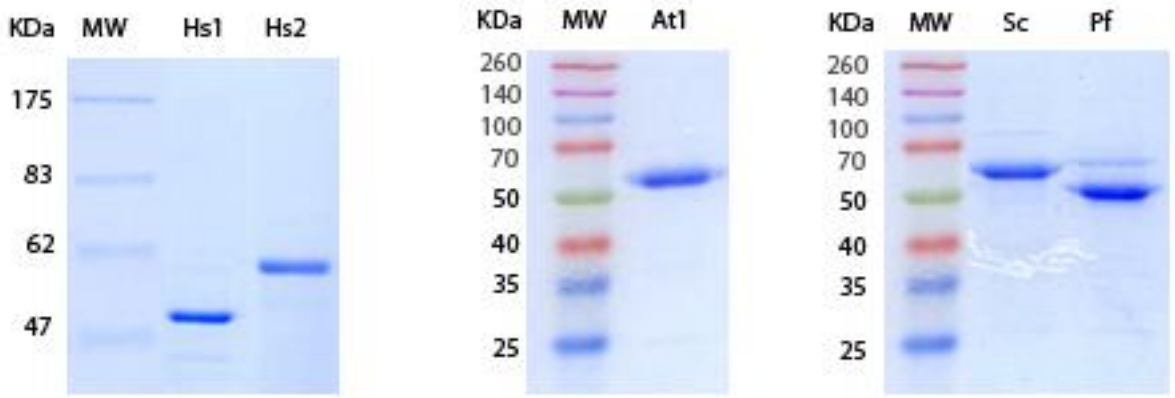
KDa
MW
Hs1
Hs2
175
83
62
47
KDa
MW
At1
260
140
100
70
50
40
35
25
KDa
MW
Sc
Pf
260
140
100
70
50
40
35
25

Fig. S1